Electron Inversion Layer Mobility Enhancement by Uniaxial Stress on (001) and (110) Oriented MOSFETs

E. Ungersboeck, V. Sverdlov, H. Kosina, and S. Selberherr
Institute for Microelectronics, TU Wien, Gußhausstraße 27–29/E360, 1040 Wien, Austria
Phone: +43-1-58801/36022, Fax: +43-1-58801/36099,
E-mail: ungersboeck@iue.tuwien.ac.at

Abstract— **The origin of the enhancement of electron mobility in inversion layers on (001) and (110) oriented Si substrates under uniaxial stress has been investigated by solving the Boltzmann equation using the Monte Carlo method. Taking into account carrier repopulation, strain induced change of intersubband scattering and of electron effective mass, the experimentally observed mobility variation under uniaxial stress can be explained. Band structure calculations were performed to quantify the influence of stress on the effective masses. The experimentally observed pronounced anisotropy of the mobility induced by uniaxial stress for both substrate orientations is well reproduced by simulations. While on (110) substrate the anisotropy stems from the ellipsoidal shape of the lowest subband ladder, an effective mass change induced by [110] stress is responsible for the anisotropic mobility on the (001) substrate.**

I. Introduction

Uniaxially stressed Si is used in leading edge logic CMOS technologies, because it can increase mobility and current drive of both n-channel and p-channel MOSFETs [1], [2], [3]. While transport in the biaxially strained Si inversion layer has often been subject to theoretical investigations, rigorous modeling of the technologically more relevant application, with process-induced uniaxial stress along the channel direction, has surprisingly been neglected until recently [4].

Theoretical modeling of strain induced mobility enhancement for electrons and holes is an important issue with some critical questions still open [5], [6], [7]. In particular, due to the uncertainty in the scattering models and parameters for the inversion layer in conjunction with the arising numerical complexity, one is forced to do severe approximations.

For this reason a phenomenological approach based on the empirically measured piezoresistance coefficients is often used by industry to predict mobility enhancement for electrons and holes [1]. However, mobility modeling based on the piezoresistance coefficients has several drawbacks: The validity of the piezoresistance coefficients is restricted to small strains and stresses ($< 500\,\mathrm{MPa}$), even though much higher values can be reached in current technologies [8]. Furthermore, in inversion layers the enhancement of the effective mobility shows a dependence on the inversion layer concentration N_s, whereas piezoresistance coefficients for the inversion layer [9] yield the mobility for only one particular N_s. Additionally, stress induced enhancement of mobility was found to depend on the body thickness of UTB MOSFETs [4], thus the piezoresistance coefficients have to be calibrated for the inversion layer concentration and the Si body thickness.

In this work a physically motivated modeling approach is presented, taking into account the effect of stress on the repopulation of subbands and subband ladders, on scattering, and on the band structure. It is shown that this model is capable of capturing the experimentally observed anisotropy of mobility enhancement $\Delta\mu$ in bulk Si and Si inversion layers. It can easily be adapted for general strain conditions, substrate orientations, and channel directions. The simulation method for the calculation of the strained Si band structure and the bulk- and inversion layer mobility is described in Section II. In Section III first the modulation of the bulk mobility by uniaxial stress is discussed. The results for the electron effective mobility in inversion layers formed on (001) and (110) substrates are summarized in Section IV.

II. Simulation Method

The band structure of Si was calculated using the non-local empirical pseudopotential method (EPM) including spin-orbit coupling [10]. Details concerning the incorporation of arbitrary strain in the band structure calculation can be found in [11]. The effective masses were extracted from the curvature of the conduction bands at the minima along various directions and have been incorporated in the transport calculations. When the strain tensor in the crystal system contains off-diagonal components, a pronounced electron effective mass change is observed. In unstrained Si the constant energy surfaces of the conduction band have a prolate ellipsoidal shape, where the semi-axes are characterized by m_l, m_t, and m_t. Here, m_l and m_t denote the longitudinal and transverse electron masses of Si, respectively. Under $\langle 110 \rangle$ stress the constant energy surfaces of the two-fold degenerate Δ_2-valleys take the form of scalene ellipsoids $(m_l, m_{t,||}, m_{t,\perp})$, where $m_{t,||}$ and $m_{t,\perp}$ denote the transverse mass parallel and perpendicular to the stress direction. Band structure simulations indicate that uniaxial tensile stress along $\langle 110 \rangle$ decreases $m_{t,||}$ with respect to $m_{t,\perp}$. Analytical fits characterizing the effective mass change of $m_l, m_{t,||}$, and $m_{t,\perp}$ as a function of applied $\langle 110 \rangle$ stress are reported in [11]. The observed effective mass change is in good agreement with a study recently reported [4].

The Monte Carlo simulator VMC [12], including fullband and analytical band models, was used to calculate the Si bulk

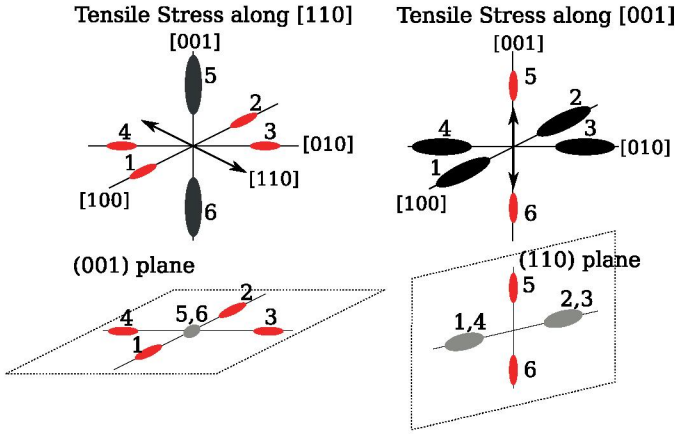

Figure 1: Constant energy surfaces of the Si conduction band under uniaxial tensile stress along [110] / [001] with projection on the (001) / (110) plane.

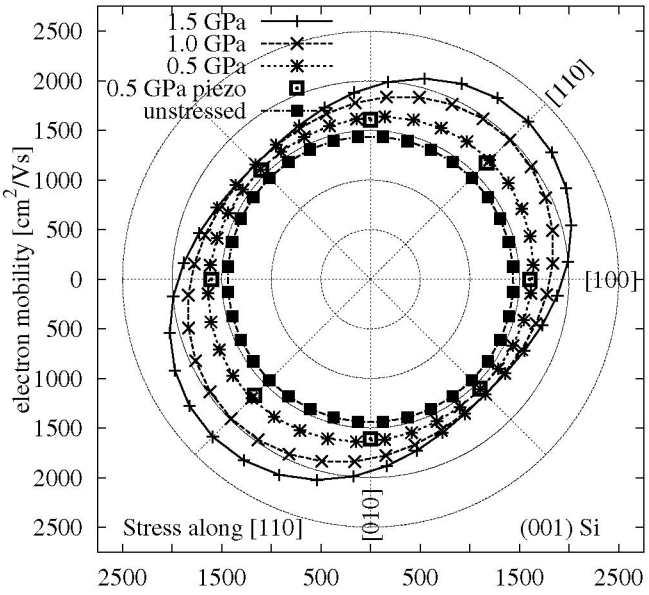

Figure 2: Simulated in-plane electron mobility for various stress levels. At 500 MPa simulation results are compared to mobility calculated from the piezoresistance coefficients (open squares).

electron mobility. The subband structure of the two dimensional electron gas was calculated using a one-dimensional Schrödinger-Poisson solver [13] with modifications to account for the strain induced energy splitting between the subband ladders. The effective mass approximation with a non-parabolicity coefficient of $\alpha = 0.5$ eV^{-1} was used for the energy dispersion of the subbands. Transport calculations have accounted for electron-phonon interaction [14] and surface roughness scattering. We use the Prange and Nee formulation [15], [16] for surface roughness scattering. Static dielectric screening is also taken into account.

The Monte Carlo method used for this work is based on the solution of the linearized Boltzmann equation and allows the exact treatment of the Pauli exclusion principle in the limit of vanishing driving fields [17].

III. Bulk Mobility Enhancement

We start the discussion with an analysis of the effect of [110] tensile stress on the electron mobility in the (001) plane, as this stress condition is commonly used in strain engineered n-channel MOSFETs. Under uniaxial tensile stress along [110] an anisotropic mobility enhancement for the (001) plane was observed experimentally [18], [19]. The anisotropy is also reflected by the linear piezoresistance coefficients [20], yielding the most pronounced mobility enhancement parallel to the stress direction.

Fig. 1 shows the constant energy surfaces of the conduction band in unstrained Si located along the six equivalent $\langle 100 \rangle$ directions. In the unstrained crystal the six valleys are equally populated, which results in an isotropic mobility. It is emphasized that a model on the basis of linear deformation potential theory alone cannot reproduce the anisotropy in the (001) plane under [110] tensile stress: According to this theory, the shift of the band minima is linearly related to the strain in the semiconductor, whereas the shape of the bands is not altered. Under tensile stress along [110], the out-of-plane valleys (labeled 5, and 6 in Fig. 1) have a higher population than the in-plane valleys (1 to 4) and will therefore mainly determine the mobility. Since, according to deformation potential theory, the energy dispersion in the out-of-plane valleys is isotropic in the (001) plane, isotropic mobility enhancement for this stress configuration is expected. This contradicts experimental observations for large stress levels.

Only when an effective mass change of the out-of-plane valleys resulting from tensile [110] stress is introduced in the simulation, can the numerical model reproduce the anisotropic mobility enhancement. The MC simulation predicts an anisotropic bulk electron mobility in the (001) plane as shown in Fig. 2 for several levels of tensile stress. At small stress a good agreement of MC results with the enhancement predicted from the piezoresistance coefficients is found (Fig. 2).

Tensile stress along [001] is favorable for electron mobility enhancement on (110) oriented substrate with the channel parallel to the stress direction. Under this stress four valleys (1 to 4) move down in energy in with respect to the valleys 5, and 6 (see Fig. 1). Similar to the (001) plane, under tensile stress along [001], the mobility becomes anisotropic in the (110) plane. The highest mobility component is observed along the [001] direction. However, band structure calculations have shown that under [001] stress the effective mass change is negligible. Thus, $\Delta\mu$ stems from the stress induced valley shifts only.

IV. Inversion Layer Mobility Enhancement

In inversion layers the six-fold degenerate Δ_6 valley splits into up to three different subband ladders depending on the orientation of the substrate. Fig. 1 shows that on (001) substrate

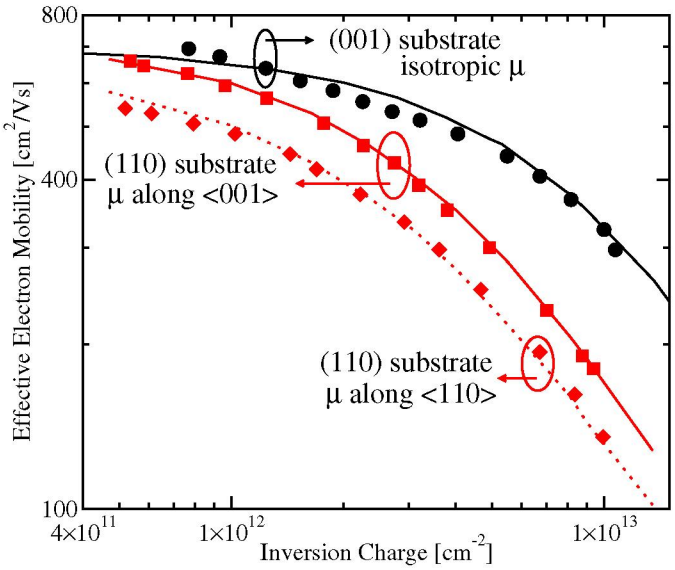

Figure 3: Simulated μ_{eff} (lines) for substrate orientation (001) and (110) compared to measurements [18], [21] (symbols). The anisotropic μ_{eff} on the (110) substrate is given along $\langle 001 \rangle$ and $\langle 110 \rangle$.

the masses of the lowest (unprimed) subband ladders (5,6) are spherical and that the ladders are two-fold degenerate. On (110) substrate the masses of the unprimed subband ladders (1 to 4) are anisotropic and the ladders are four-fold degenerate. The higher density of states and larger transport masses on (110) substrate yield a lower inversion layer mobility as compared to (001) substrate. This can be seen in Fig. 3, where we compare experimental data [18], [21] to MC simulation results.

A. Mobility enhancement for (001) oriented substrate

In Fig. 4 the effective mobility components parallel and perpendicular to stress direction [110] for two tensile stress levels are compared to the unstrained mobility. Tensile stress along [110] has two beneficial effects on the parallel mobility component: The splitting between the unprimed and primed ladders is increased, and the transport mass in direction of the stress is reduced with respect to the unstrained case. From these two effects one can understand the mobility enhancement parallel to the stress direction at all inversion layer densities. Perpendicular to stress, the effective mass is increased by stress, leading to a smaller mobility enhancement in this direction. Additionally, in Fig. 5 the relative mobility enhancement for [110] stressed (001) oriented substrate is plotted as a function of the in-plane angle at two levels of stress. The mobility is enhanced at all angles, with the largest mobility enhancement parallel to the stress direction. The pronounced anisotropy at large stress is solely a result of the effective mass change and is in good agreement with experimental data [19].

For (001) oriented substrate the in-plane effective mass change of electrons under biaxial tensile stress, was found to be small as compared to uniaxially [110] stressed Si [11].

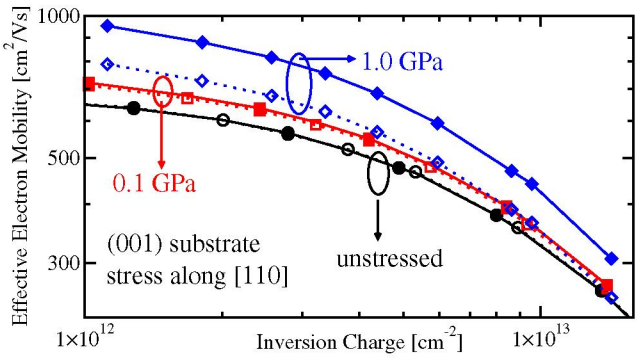

Figure 4: Simulated mobility parallel (closed symbols) and perpendicular (open symbols) to stress direction [110] with no stress (circles), 0.1 GPa (squares), and 1.0 GPa stress (diamonds).

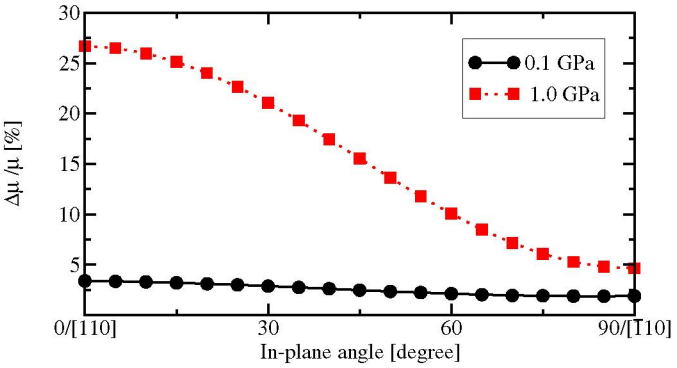

Figure 5: Anisotropic mobility enhancement for (001) substrate with tensile stress along [110] at $N_{\text{s}} = 5 \cdot 10^{12}$ cm^{-2}.

While mobility enhancement in biaxially stressed Si is saturating at a stress of 1 GPa, a saturation of mobility enhancement is not expected for uniaxially [110] stressed Si, as the effective mass change is not saturating as a function of stress [4], [11].

If stress is parallel to [100], the influence of uniaxial stress on the subband ladders is different from substrate with stress along [110]: Stress along [100] lifts the degeneracy of the four-fold (primed) ladder. Since the stress induced effective mass change is small, $\Delta\mu_{\text{eff}}$ is a result of subband ladder repopulation only, thus, like for biaxially strained Si, a saturation of the mobility enhancement is expected around 1 GPa.

B. Mobility enhancement for (110) oriented substrate

To enhance the mobility for (110) substrate a uniaxial tensile stress along [001] is advantageous, as this stress condition increases the splitting between the unprimed and primed ladder. From EPM simulations we get only a negligible change of the effective masses which determine the transport in the subband ladders for this stress condition. Hence, the stress induced mobility change is attributed to repopulation between unprimed and primed subband ladders and to suppressed inter-subband scattering. From Fig. 6 we observe that stress

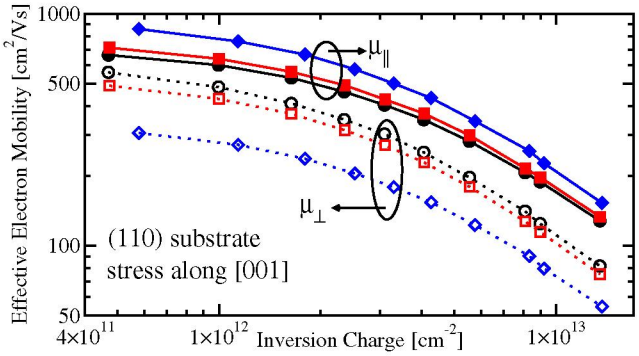

Figure 6: Simulated mobility parallel (closed symbols) and perpendicular (open symbols) to stress direction [110] with no stress (circles), 0.1 GPa (squares), and 1.0 GPa stress (diamonds).

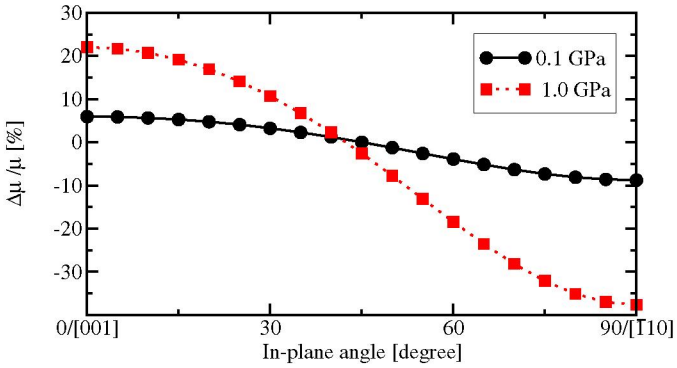

Figure 7: Anisotropic mobility enhancement for (110) substrate with tensile stress along [001] at $N_s = 5 \cdot 10^{12}$ cm^{-2}.

increases μ_{eff} parallel to the stress direction, whereas the mobility perpendicular to the stress direction is smaller compared to the unstressed case. Since no effective mass change occurs, the mobility change is expected to saturate at larger stress ($\sim$ 1 GPa), as soon as the primed ladder becomes depopulated.

The stress induced mobility enhancement is shown in Fig. 7 as a function of the in-plane angle at two levels of stress. It is apparently different from the dependence observed for [110] stressed (001) substrate. For (110) substrate and tensile [110] stress a mobility enhancement parallel to the stress direction is observed, while the mobility perpendicular to the stress direction is reduced. Again, these findings are supported by experimental results [19].

V. Conclusions

Electron inversion layer mobility was analyzed by means of MC simulations. Experimentally observed mobility data [4], [19], [21] were reproduced for bulk Si and Si inversion layers on (001) and (110) oriented substrates. Mobility enhancement can be understood from a combination of three effects: (i) valley (subband ladder) repopulation, (ii) change in inter-valley, inter-subband scattering, and (iii) stress induced effective mass changes. Under stress along $\langle 110 \rangle$ solely the change in the electron effective mass, extracted from EPM band structure calculations, can explain the experimentally observed anisotropic mobility enhancement.

Acknowledgement

This work has been partly supported by the Austrian Science Fund (FWF), projects 17285-N02 and I79-N16.

References

[1] S.-E. Thompson *et al.*, IEEE Trans.Electron Devices **51**, 1790 (2004).

[2] M. Horstmann, A. Wei, and T. Kammler, in *Proc. Intl. Electron Device Meeting* (2005), pp. 233–236.

[3] C.-H. Jan, P. Bai, and J. Choi, in *Proc. Intl. Electron Device Meeting* (2005), pp. 60–63.

[4] K. Uchida, T. Krishnamohan, K. Saraswat, and Y.Nishis, in *Proc. Intl. Electron Device Meeting* (2005), pp. 135–138.

[5] M. V. Fischetti, F. Gamiz, and W. Hänsch, J.Appl.Phys. **92**, 7320 (2002).

[6] M. V. Fischetti and Z. Ren, J.Appl.Phys. **94**, 1079 (2003).

[7] E. Ungersboeck and H. Kosina, in *Proc. Simulation of Semiconductor Processes and Devices* (Tokio, Japan, 2005), pp. 311–314.

[8] L. Washington *et al.*, IEEE Electron Device Lett. **27**, 511 (2006).

[9] S.-E. Thompson, G. Sun, Y. Choi, and T. Nishida, IEEE Trans.Electron Devices **53**, 1010 (2006).

[10] M. M. Rieger and P. Vogl, Phys. Rev. B **48**, 14276 (1993).

[11] E. Ungersboeck *et al.*, in *11th International Workshop on Computational Electronics Book of Abstracts* (2006), pp. 141–142.

[12] http://www.iue.tuwien.ac.at/software, *VMC 2.0 User's Guide*, Institut für Mikroelektronik, Technische Universität Wien, Austria, 2006.

[13] D. Vasileska and Z. Ren, *SCHRED 2.0 User's Manual*, http://www.nanohub.org, (2000).

[14] C. Jacoboni and L. Reggiani, Reviews of Modern Physics **55**, 645 (1983).

[15] R. Prange and T. Nee, Phys.Rev. **168**, 779 (1968).

[16] D. Esseni, IEEE Trans.Electron Devices **51**, 394 (2004).

[17] S. Smirnov, H. Kosina, M. Nedjalkov, and S. Selberherr, J.Appl.Phys. **94**, 5791 (2003).

[18] K. Uchida, J. Koga, and S. Takagi, in *Proc. Intl. Electron Device Meeting* (2003), pp. 805–808.

[19] H. Irie, K. Kita, K. Kyuno, and A. Toriumi, in *Proc. Intl. Electron Device Meeting* (2004), pp. 225–228.

[20] C. S. Smith, Phys. Rev. **94**, 42 (1954).

[21] G. Tsutsui *et al.*, in *Proc. Intl. Electron Device Meeting* (2005), pp. 747–750.